

Inductive acceleration of ions in Poynting-flux dominated outflows

JOHN G. KIRK¹ AND GWENAEL GIACINTI¹

¹*Max-Planck-Institut für Kernphysik, Postfach 103980, 69029 Heidelberg, Germany*

(Accepted for publication in the *Astrophysical Journal*)

ABSTRACT

Two-fluid (electron-positron) plasma modelling has shown that inductive acceleration can convert Poynting flux directly into bulk kinetic energy in the relativistic flows driven by rotating magnetized neutron stars and black holes. Here, we generalize this approach by adding an ion fluid. Solutions are presented in which all particles are accelerated as the flow expands, with comparable power channeled into each of the plasma components. In an ion-dominated flow, each species reaches the limiting rigidity, according to Hillas' criterion, in a distance significantly shorter than in a lepton-dominated flow. These solutions support the hypothesis that newly born magnetars and pulsars are potential sources of ultra-high energy cosmic rays. The competing process of Poynting flux dissipation by magnetic reconnection is shown to be ineffective in low-density flows in which the conventionally defined electron multiplicity satisfies $\kappa_e \lesssim 10^5 (4\pi L_{38}/\Omega)^{1/4} / \text{Max}(\eta_{\text{ion}}^{1/2}, 1)$, where $L_{38} \times 10^{38} \text{erg s}^{-1}$ is the power carried by the flow in a solid angle Ω , and η_{ion} is the ratio of the ion to lepton power at launch.

Keywords: acceleration of particles — galaxies: jets — plasmas — pulsars: general — shock waves — stars: winds, outflows

1. INTRODUCTION

Newly born magnetars, rapidly rotating pulsars and rotating black holes, are thought to drive relativistic outflows that are dominated by Poynting flux. They have long been recognized as promising candidate sources of ultra-high energy cosmic rays (for a review see [Kotera & Olinto 2011](#)), and have recently been suggested as sources of PeV neutrinos ([IceCube Collaboration et al. 2018](#)). However, the physics of the particle acceleration processes at work remains uncertain (see, for example, the discussion in [Lemoine 2013](#)), and most theoretical work has concentrated on the problem of accelerating the leptons needed to explain the highly variable gamma-ray emission that has been attributed to these objects.

For example, “inductive acceleration”, was advanced by [Kirk & Giacinti \(2017\)](#) as an explanation of the gamma-ray flares observed from the Crab Nebula ([Bühler & Blandford 2014](#)). It involves gradually extracting energy from the fluctuating component of the magnetic field in a Poynting-flux dominated, electron-positron outflow as it propagates radially, undisturbed by the surrounding medium ([Kirk & Mochol 2011a,b](#)). In the case of the Crab, acceleration by this process is limited because the pulsar wind terminates at about

4×10^{17} cm from the pulsar, at which point only 10% of the available energy has been channeled into relativistic particles. Nevertheless, the mechanism injects leptons of several PeV into the surrounding nebula.

Motivated by the renewed interest in the acceleration of hadrons in Poynting-flux dominated outflows (e.g., [Petropoulou & Mastichiadis 2018](#); [Werner et al. 2018](#); [Alves et al. 2018](#); [Reimer et al. 2018](#); [Gao et al. 2019](#); [Zacharias et al. 2019](#)), this paper generalizes inductive acceleration to outflows that contain a significant component of ions. We find that ions are indeed accelerated to high energy, that they are inevitably accompanied by a comparable flux of high energy leptons, and that they alleviate one of the main limitations of purely leptonic flows by substantially speeding up the acceleration process.

The fundamental assumption underlying inductive acceleration is that the central object launches a relativistic, Poynting-flux dominated flow, that can be considered to be radial and uniform within a given solid angle. The analysis starts at a radius where the particle density is high enough for the equations of ideal MHD to apply. The flow is assumed to have negligible thermal pressure at this point, and to be causally detached from the central object, in the sense that its velocity exceeds that of a radially propagating fast magnetosonic wave. We

show that the MHD description fails beyond a certain radius, because the plasma density decreases outwards. Short length-scale variations in the toroidal magnetic field that are frozen into the MHD flow, then gradually convert their Poynting flux into radial bulk motion of the plasma. This continues until all small-scale structure is erased, unless the flow previously terminates by encountering an external medium. In § 2 we motivate our assumptions and discuss the nature of the frozen-in fluctuations. The fluid equations that include ions are presented in § 3. Approximate analytic formulas describing the different phases of the flow are given and illustrated using numerical solutions of the underlying equations in § 4. The physical interpretation of the solutions and their range of validity is discussed in more depth in § 5, where the mechanism is compared and contrasted with the related processes of reconnection and unipolar induction. Our conclusions are summarized in § 6.

2. POYNTING FLUX DOMINATED OUTFLOWS

As is well-known (Buckley 1977), the force-free MHD equations for a steady, axisymmetric flow imply radial acceleration of its constituent charges such that their Lorentz factor increases linearly with radius r and the magnetization parameter σ , which is the ratio of the radial Poynting flux to the radial kinetic energy flux, decreases inversely with r (Contopoulos et al. 1999; Contopoulos & Kazanas 2002; Arons 2003). Bogovalov (1999) showed this property holds also for non-axisymmetric flows that contain reversals of the magnetic field, provided these are concentrated in current sheets of thickness small compared to r . However, the force-free approximation neglects the inertia of the particle component of the wind, which becomes increasingly important towards larger radius, and the solution loses its validity when the Lorentz factor of the flow approaches that of the fast magnetosonic wave. Exactly where this happens depends on how particles are injected into the flow. In the idealized case of a cold axisymmetric wind, the fast magnetosonic point retreats to infinite radius (Michel 1969; Goldreich & Julian 1970). But, at least for pulsars, this is probably irrelevant, since models of pair production suggest particles are injected with Lorentz factors $\sim 10^2$ to 10^3 , in which case the flow is supersonic already relatively close to the star (Lyubarsky & Kirk 2001), i.e., near the “light cylinder” at $r = r_L (= cP/2\pi)$, where P is the pulsar period).

Beyond the fast-magnetosonic point, acceleration must quickly cease, since the plasma cools adiabatically, and a cold, radial, supersonic flow that obeys the ideal MHD equations, propagates at constant γ and

σ (for a review, see Kirk et al. (2009)). In this phase of the flow, the field reversals considered by Bogovalov (1999) become concentric current sheets separating regions of toroidal magnetic field with opposite polarity — a “striped wind”. However, any fluctuations in the toroidal field that appear in the co-moving frame to be static, local equilibria are frozen into the flow and are convected radially with it.

As the plasma thins out further, a radius is reached at which also the ideal MHD approximation fails. For relatively high particle densities, this can happen if dissipation becomes important, for example, in the guise of reconnection (see Coroniti (1990), Lyubarsky & Kirk (2001), Drenkhahn & Spruit (2002), Kirk & Skjæraasen (2003), and the discussion in § 5.1). But, even without dissipation, the MHD approximation fails when the inertia associated with the plasma current — which is essential to preserve the frozen-in fluctuations — becomes important (Usov 1975).

This effect was examined by Kirk & Mochol (2011a) (“KM” in the following), who used a perturbation method to formulate equations governing the radial evolution of an electron-positron wind with a frozen-in, sheared magnetic field, assuming each lepton species can be described as a cold fluid. The main difference between this approach and those based on dissipation, is that the local equilibrium in the MHD flow is not assumed to be a pressure-supported structure, such as a hot current sheet, but is, instead, a force-free equilibrium. This relieves the problems associated with postulating that dissipation leads to an isotropic particle velocity distribution, which can be shown to be physically inconsistent beyond a critical, density-dependent, radius — see § 5 and Lyubarsky & Kirk (2001).

The particular force-free equilibrium chosen by KM is a “sheet-pinch” (Bobrova et al. 2001; Li et al. 2003), with constant rate of shear. Subsequently, a configuration with two field reversals per wave period, concentrated in rotational discontinuities, was examined by Kirk & Giacinti (2017). Here, we generalize two aspects of these treatments. Firstly, we show that the precise structure of the equilibrium, in particular the thickness of the current-carrying layers, is not important for the large-scale evolution of the flow. Secondly, and more importantly, we examine the consequences of adding a fluid of cold ions to the flow, assuming they do not contribute to the transverse current and that their charge density is compensated by an excess of electrons over positrons.

3. THE MULTI-FLUID EQUATIONS

We consider solutions of the multi-fluid equations that depend spatially only on r , contain a transverse component of the magnetic field that oscillates in the lab. frame with angular frequency $\omega = c/r_L \gg c/r$ and are, to zeroth order in r_L/r , stationary in a frame comoving radially with the wave. Following KM, we denote the radial component of the four-speed (in units of c) of fluid s ($s = e, i, p$ for electrons, ions and positrons, respectively) by $p_{\parallel s}$, and use the complex quantity $p_{\perp s}$ to denote the two components transverse to the radius vector. Since the radial component of the three-speed of each charged fluid species equals the pattern speed $c\beta_w$ of the wave, one has

$$p_{\parallel s} = \beta_w \gamma_s, \quad (1)$$

where

$$\begin{aligned} \gamma_s &= \sqrt{1 + p_{\parallel s}^2 + |p_{\perp s}|^2} \\ &= \gamma_w \sqrt{1 + |p_{\perp s}|^2}, \end{aligned} \quad (2)$$

and $\gamma_w = (1 - \beta_w^2)^{-1/2}$ is the Lorentz factor of the wave. KM considered a purely leptonic flow, in which case, the electron and positron flows can be assumed to be symmetric in velocity: $p_{\parallel e} = p_{\parallel p}$ and $p_{\perp e} = -p_{\perp p}$, and have equal proper densities: $n_e = n_p$. Here we add a fluid containing ions of charge Ze , assuming (i) it does not contribute to the transverse current, i.e., $p_{\perp i} = 0$, (ii) it does not affect the symmetry of the electron-positron velocities, and (iii) its charge density is compensated by an excess of electrons, such that the flow remains neutral in the lab. frame: $Zn_i = \gamma_e(n_e - n_p)/\gamma_i$. As discussed in 3.2, we assume $|p_{\perp s}|$ is independent of wave phase. It then follows from (1) that $p_{\parallel s}$ is also phase-independent, and the rate of shear is determined by the phase-dependence of the proper densities.

3.1. Conservation of particle number

The continuity equation for the zeroth order quantities in the case of electron and positron fluids is given in KM, Eq. (14), (henceforth, we refer to equations in KM as (KM 14), etc.). To account for the presence of ions, we introduce the constant η_{ion} , which equals the ratio of the rest-mass flux carried by ions to that carried by leptons. (At launch, η_{ion} equals the ratio of the power carried by ions to that carried by leptons — a quantity that evolves as the flow accelerates.) The continuity equation (KM 14) then becomes:

$$(1 + \eta_{\text{ion}}) \frac{r^2 p_{\parallel e} \omega_p^2}{r_L^2 \omega^2} = a_{Le}^2 / \mu, \quad (3)$$

where the proper plasma frequency is defined as

$$\omega_p = [4\pi \langle n_e + n_p \rangle e^2 / m_e]^{1/2}, \quad (4)$$

and $\langle \dots \rangle$ denotes a phase average. The right-hand side of Eq. (3) is $4\pi e^2 / (m_e^2 c^3)$ times the phase-averaged flux of rest-mass per unit solid angle, $d\dot{M}/d\Omega$, expressed in terms of the following dimensionless constants:

1. The “strength” parameter

$$\begin{aligned} a_{Le} &= [4\pi (dL/d\Omega) e^2 / m_e^2 c^5]^{1/2} \\ &= 3.4 \times 10^{10} (4\pi L_{38} / \Omega)^{1/2}, \end{aligned}$$

with $dL/d\Omega$ the power per unit solid angle carried by the flow, and L_{38} the corresponding total power expressed in units of $10^{38} \text{ erg s}^{-1}$, assuming the flow occupies an effective solid angle Ω . In electron-positron plasmas, a_{Le} is a characteristic value of the maximum leptonic Lorentz factor. More generally, the parameter $a_{Ls} = (|q_s| m_e / e m_s) a_{Le}$ gives the characteristic maximum Lorentz factor for particles of species s . In Poynting-flux dominated flows, the magnitude of the toroidal magnetic field, $|B|$, is inversely proportional to r , and a_{Ls} equals the ratio of the gyro frequency of a (nonrelativistic) particle of species s to the wave frequency, when the fields are extrapolated back to radius r_L :

$$\begin{aligned} a_{Ls} &= |q_s B| r / (m_s c^2) \\ &= |q_s B_L| / (m_s c \omega) \end{aligned} \quad (5)$$

2. The inverse mass-loading:

$$\mu = (dL/d\Omega) / (c^2 d\dot{M}/d\Omega), \quad (6)$$

where $d\dot{M}/d\Omega$ is the rest-mass flux per unit solid angle. In a pure lepton model, μ equals the Lorentz factor that would be achieved by the flow after conversion of the entire electromagnetic energy flux into kinetic energy.

As an alternative to μ , a more intuitive measure of the rest-mass flux is the particle multiplicity κ_s at $r = r_L$. This quantity is conventionally defined as the ratio of the lab. frame charge density to the “Goldreich-Julian” charge density $B_L \omega / 2\pi c$, where B_L is the magnitude of the toroidal magnetic field, extrapolated back to radius r_L (Lyubarsky & Kirk 2001). For an electron-positron plasma, $\kappa_e = a_{Le} / (4\mu)$ (see KM 7). Adding an ion fluid, and introducing the notation κ_{ep} for the sum of the electron and positron multiplicities leads to

$$\begin{aligned} \kappa_{ep} &= \kappa_e + \kappa_p \\ &= a_{Le} / [2\mu (1 + \eta_{\text{ion}})]. \end{aligned} \quad (7)$$

The ion multiplicity follows from the condition of charge neutrality, $\kappa_i = \kappa_e - \kappa_p$, and can also be expressed in terms of η_{ion} :

$$\kappa_i = \kappa_{\text{ep}} \eta_{\text{ion}} Z m_e / m_i. \quad (8)$$

Equation (3), can then be reformulated using (1) and (2) to give an expression for the plasma frequency as a function of r , p_\perp and γ_w (or, equivalently, β_w):

$$\omega_p^2 = \frac{2\kappa_{\text{ep}} c^2 a_{\text{Le}}}{r^2 \beta_w \gamma_w \sqrt{1 + p_\perp^2}}, \quad (9)$$

where $p_\perp = |p_{\perp e}| = |p_{\perp p}|$.

3.2. Ampère's Law

Seen from the comoving frame, the flow is locally in force-free equilibrium, with the transverse components of the electron and positron four-speeds, and, therefore, the plasma current, directed along the local magnetic field. Then, in the absence of plasma pressure, the (complex) transverse magnetic field B simply rotates as a function of wave phase, φ , keeping its magnitude constant to zeroth order. This behavior follows from Ampère's law, which links the (complex) transverse current density j_\perp with B according to (KM 13):

$$\begin{aligned} \frac{\partial B}{\partial \varphi} &= \frac{4\pi i j_\perp \beta_w \gamma_w^2}{\omega} \\ &= \frac{4\pi i (p_{\perp p} n_p - p_{\perp e} n_e) e c \beta_w \gamma_w^2}{\omega}. \end{aligned} \quad (10)$$

Integrating this equation over a phase interval in which B reverses its sign one finds

$$\int_{\text{reversal}} d\varphi |j_\perp| = (|B|/\gamma_w) / (4\beta_w \gamma_w / \omega). \quad (11)$$

(Note that $|B|/\gamma_w$ is the amplitude of the magnetic field in the frame co-moving with the wave, and $2\pi c \beta_w \gamma_w / \omega$ is the wavelength in this frame.)

Equation (11) allows some freedom in specifying the phase-dependencies of the transverse fluid velocities and densities. For simplicity, we treat here the case where $|p_{\perp e}| = |p_{\perp p}|$ is constant, and the entire phase-dependence of the amplitude of the current arises from that of the density. Then, assuming two, not necessarily thin, field reversals per wave period, the averaged proper particle densities $\langle n_{e,p} \rangle = \int_0^{2\pi} n_s d\varphi / (2\pi)$ obey:

$$\int_{\text{reversal}} d\varphi |j_\perp| = e c p_\perp \pi \langle n_e + n_p \rangle \quad (12)$$

so that, from (11), and (4),

$$|B| = \frac{m_e c \beta_w \gamma_w^2 p_\perp \omega_p^2}{e \omega}. \quad (13)$$

Eliminating ω_p using the continuity equation (9) gives:

$$|B| = \frac{m_e c^3 2\kappa_{\text{ep}} a_{\text{Le}} p_\perp \gamma_w}{e \omega r^2 \sqrt{1 + p_\perp^2}}. \quad (14)$$

3.3. Conservation of energy

The equation of conservation of energy can be written as

$$\mu = \Psi_{\text{Poynting}} + \Psi_{\text{particle}} \quad (15)$$

where, Ψ_{Poynting} is the normalized Poynting flux:

$$\Psi_{\text{Poynting}} = \frac{\beta_w r^2 |B|^2}{4\pi c \left(d\dot{M}/d\Omega \right)} \quad (16)$$

and Ψ_{particle} is the normalized kinetic energy flux:

$$\Psi_{\text{particle}} = r^2 \sum m_s c \langle n_s \rangle \gamma_s p_{\parallel s} / \left(d\dot{M}/d\Omega \right). \quad (17)$$

(see (KM A26)). The purely leptonic case is particularly simple, since the energy flux carried by particles is just $\gamma_e c^2$ times the particle rest-mass flux. In terms of the magnetization parameter, $\sigma = \Psi_{\text{Poynting}}/\Psi_{\text{particle}}$, one then finds (KM 15) $\mu = \gamma_e (1 + \sigma)$. In the presence of ions, however, this equation is modified because the ion energy flux is $\gamma_w c^2$ times the ion rest-mass flux, whereas the leptonic energy flux is $\gamma_e c^2$ times the leptonic rest-mass flux, so that

$$\begin{aligned} \Psi_{\text{Poynting}} &= \frac{\mu \beta_w}{a_{\text{Le}}^2} \left(\frac{e r |B|}{m_e c^2} \right)^2 \\ &= \frac{2\kappa_{\text{ep}} a_{\text{Le}} r_\perp^2}{(1 + \eta_{\text{ion}})} \left(\frac{\beta_w \gamma_w^2 p_\perp^2}{r^2 (1 + p_\perp^2)} \right) \end{aligned} \quad (18)$$

and

$$\Psi_{\text{particle}} = \left(\frac{\eta_{\text{ion}} + \sqrt{1 + p_\perp^2}}{1 + \eta_{\text{ion}}} \right) \gamma_w. \quad (19)$$

where, in (18), Ampère's equation (14) was used to eliminate $|B|$. With these definitions, (15) is an algebraic equation relating the r -dependent variables p_\perp and γ_w .

3.4. Radial momentum balance equation

The radial momentum flux per unit mass, ν , is similar in form to the normalized energy flux μ in Eq. (15):

$$\nu = \Pi_{\text{Poynting}} + \Pi_{\text{particle}} \quad (20)$$

where Π_{Poynting} is the normalized electromagnetic momentum flux per unit solid angle:

$$\Pi_{\text{Poynting}} = \left(\frac{1 + \beta_w^2}{2\beta_w} \right) \Psi_{\text{Poynting}} \quad (21)$$

and Π_{particle} is the particle contribution:

$$\Pi_{\text{particle}} = \beta_w \Psi_{\text{particle}} \quad (22)$$

However, radial momentum is not conserved. In the purely leptonic case, this leads to equation (KM 16), the right-hand side of which is modified by the presence of ions (cf. KM A27) to give:

$$\begin{aligned} \frac{d\nu}{dr} &= \frac{\mu r p_{\perp}^2 \omega_p^2}{a_{\text{Le}}^2} \\ &= \frac{p_{\perp}^2}{(1 + \eta_{\text{ion}}) \beta_w \gamma_w r \sqrt{1 + p_{\perp}^2}} \end{aligned} \quad (23)$$

In principle, this first-order, ordinary differential equation for the zeroth-order functions p_{\perp} and γ_w closes the system, when combined with the algebraic constraint (15) and the definitions (18) and (19). However, for a relativistic flow, $\Psi_{\text{Poynting}} \approx \Pi_{\text{Poynting}}$ and $\Psi_{\text{particle}} \approx \Pi_{\text{particle}}$. Because of this, it is preferable to reformulate (23) by subtracting the conserved energy flux from the momentum flux (times c). Expanding ν and μ in $1/\gamma_w$, one then arrives at the radial momentum balance equation:

$$\begin{aligned} \frac{d}{dr} \left[\frac{\kappa_{\text{ep}} a_{\text{Le}} r_{\text{L}}^2 p_{\perp}^2}{4r^2 \gamma_w^2 (1 + p_{\perp}^2)} - \frac{\eta_{\text{ion}} + \sqrt{1 + p_{\perp}^2}}{2\gamma_w} \right] \\ = \frac{p_{\perp}^2}{r \gamma_w \sqrt{1 + p_{\perp}^2}}, \end{aligned} \quad (24)$$

which is used in place of (23) to determine the solutions described below.

4. PROPERTIES OF THE SOLUTIONS

It is a good approximation to set $\beta_w = 1$ when inserting expression (18) for the Poynting flux into the energy equation (15), since the flows we consider are everywhere relativistic. This results in a quadratic equation, which can be solved to give γ_w as a function of r and p_{\perp} . The radial momentum balance equation (24) then reduces to a first-order ordinary differential equation for p_{\perp} as a function of r , which is easily integrated using a standard algorithm. However, several key properties of the outflow can be deduced purely analytically.

If Poynting flux dominates and the flow is relativistic, it follows from energy conservation (15) and (18) that

$$\gamma_w \approx \frac{r \sqrt{1 + p_{\perp}^2}}{2\kappa_{\text{ep}} r_{\text{L}} p_{\perp}}. \quad (25)$$

Therefore, in the MHD phase, where $p_{\perp} \ll 1$ and γ_w is constant, one has $p_{\perp} \propto r$, which demonstrates explicitly that the MHD approximation fails at a critical radius.

Furthermore, beyond this radius, where $p_{\perp} \gtrsim 1$, the flow must enter an acceleration phase with $\gamma_w \propto r$, which persists until the kinetic energy flux becomes comparable in magnitude to the Poynting flux. This conclusion holds for both purely leptonic flows and for flows containing ions.

The critical radius, r_{MHD} , at which MHD fails can then be estimated from (25) to be

$$\begin{aligned} r_{\text{MHD}} &\approx \sqrt{2} r_{\text{L}} \kappa_{\text{ep}} \gamma_{w0} \\ &= 2^{1/6} r_{\text{L}} \left(\frac{a_{\text{Le}} \mathcal{M}^2 \kappa_{\text{ep}}^2}{1 + \eta_{\text{ion}}} \right)^{1/3} \\ &= 3.6 \times 10^3 r_{\text{L}} \left(\frac{\mathcal{M}^2 \kappa_{\text{ep}}^2}{1 + \eta_{\text{ion}}} \right)^{1/3} \left(\frac{4\pi L_{38}}{\Omega} \right)^{1/6} \end{aligned} \quad (26)$$

where $\mathcal{M} = \gamma_{w0}/\sigma_0^{1/2} = \gamma_{w0}^{3/2}/\mu^{1/2} \gtrsim 1$ is the relativistic Mach number of the flow at launch, at which point $\gamma_w = \gamma_{w0}$ and $\sigma = \sigma_0$.

The properties of these flows are illustrated by the examples presented in Fig. 1, which depicts numerical solutions, obtained using *Mathematica*, of Eqs. (24) and (15), for both a pure electron-positron plasma (left-hand panel) and a plasma containing also protons (right-hand panel), assuming that the two current layers are symmetrically located in wave phase, i.e., that the phase-averaged magnetic field vanishes. (It is straightforward to lift this assumption, see Kirk & Giacinti (2017).) In each case, three regimes can be identified: (i) a mildly supersonic MHD flow extending from the launching point to $r \approx r_{\text{MHD}}$, in which the Lorentz factors of the fluids are approximately constant and equal to that of the pattern γ_w , (ii) an acceleration phase at $r_{\text{MHD}} < r < r_{\text{max}}$, (see Eq. (33)) during which $\gamma_w \propto r$, and the Poynting flux steadily decreases, and (iii) a coasting phase at $r > r_{\text{max}}$, where the plasma relaxes to an outflow with all species moving radially at the same, constant Lorentz factor, and vanishingly small Poynting flux.

The main feature that distinguishes ion-carrying flows from pure electron-positron flows is the rapid energization of the leptons at the beginning of the acceleration phase. The transverse velocity of the leptons initially rises, and then stabilizes at a value $p_{\perp \text{Leq}} > 1$ that remains constant until the end of the acceleration phase at $r \approx r_{\text{max}}$. This arises because the radial acceleration of the ion fluid must equal that of the lepton fluids. In the case of the ions, radial acceleration is provided by the phase-averaged effect of the first-order, radial electric fields, which, since the plasma is neutral, extract the same momentum from the lepton fluids. However, the leptons over-compensate by acquiring signifi-

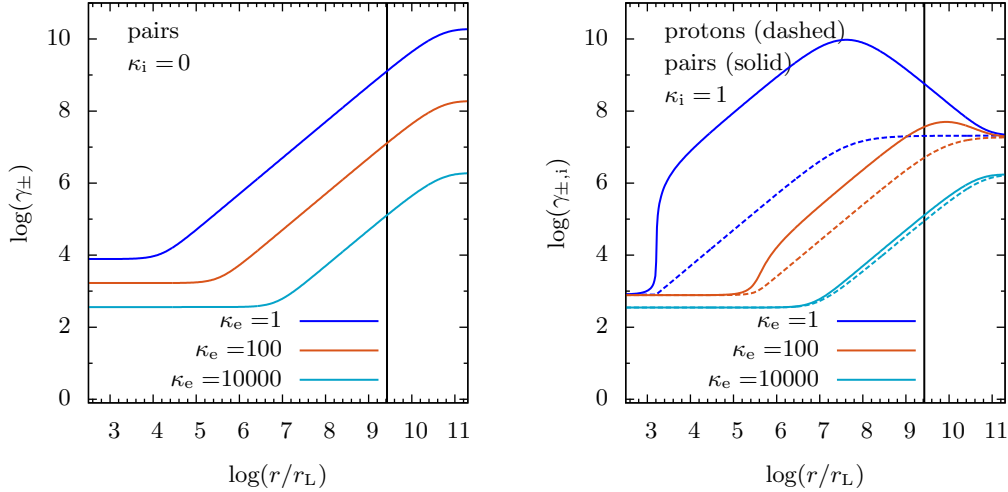


Figure 1. Numerical integration of the multi-fluid equations for a pure electron-positron plasma, with $\kappa_i = 0$, (left-hand panel), and for a plasma containing also a proton fluid with $\kappa_i = 1$, (right-hand panel), for electron multiplicities $\kappa_e = 1$, 10^2 , and 10^4 , corresponding, in the right-hand panel, to $\eta_{\text{ion}} = 1836$, 9.2 and 0.09 , respectively. In each case the strength parameter $a_{Le} = 7.6 \times 10^{10}$, appropriate for the wind of the Crab pulsar, and the flow is launched at Mach number $\mathcal{M} = 5$. The vertical black line indicates the location of the termination shock in the Crab Nebula (in which $r_L = 1.6 \times 10^8$ cm).

cant toroidal momentum, thereby enhancing the $\vec{j}_\perp \wedge \vec{B}$ and the centrifugal terms in their radial equation of motion, both of which are of first order, since the current is closely aligned to the magnetic field, and the centrifugal force is inversely proportional to the radius.

In both the MHD and the acceleration zones, Poynting flux dominates the flow, and one can use (25) to simplify the radial momentum balance equation (24):

$$\frac{dp_\perp}{dr} = \frac{p_\perp (1 + p_\perp^2)}{r} \times \left[\frac{1 - p_\perp^2 + \eta_{\text{ion}} \sqrt{1 + p_\perp^2} - \frac{4\kappa_{\text{ep}}^2 a_{Le} r_L^3 p_\perp^3}{r^3 (1 + p_\perp^2)}}{(1 + p_\perp^2)^2 + \eta_{\text{ion}} \sqrt{1 + p_\perp^2} - \frac{4\kappa_{\text{ep}}^2 a_{Le} r_L^3 p_\perp^3}{r^3 (1 + p_\perp^2)}} \right] \quad (27)$$

In the acceleration zone, the terms arising from Poynting flux (those containing a_{Le}) are negligible, and one finds that p_\perp saturates at

$$p_{\perp\text{eq}} = \left(\eta_{\text{ion}}^2 + \eta_{\text{ion}} \sqrt{\eta_{\text{ion}}^2 + 8} + 2 \right)^{1/2} / \sqrt{2}. \quad (28)$$

I.e., $p_{\perp\text{eq}} \approx 1$ in a pair-dominated flow ($\eta_{\text{ion}} \ll 1$) and $p_{\perp\text{eq}} \approx \eta_{\text{ion}}$ in an ion dominated flow ($\eta_{\text{ion}} \gg 1$). Since the lepton Lorentz factors in the acceleration phase are $\gamma_e = \gamma_p = \gamma_w \sqrt{1 + p_\perp^2}$, a flow in which ions dominate the rest-mass flux, achieves equipartition between the energy fluxes carried by ions and leptons in the acceleration phase.

Another feature of flows containing ions is that the radius at which acceleration sets in decreases as η_{ion} increases, as indicated by Eq. (26). This, together with

the rapid energization described above, causes the maximum Lorentz factor to be reached much sooner than in purely leptonic flows. For example, Fig 1 shows that when $\kappa_i = 1$, $\kappa_e = 1$ and $\eta_{\text{ion}} = 1836$ (corresponding to protons), the acceleration starts at roughly $4 \times 10^3 r_L$ and ends at $10^8 r_L$ — in the case of the Crab, well before the termination shock is reached. On the other hand, for protons with $\kappa_i = 1$, in a wind with $\kappa_e = 10^4$, there is essentially no deviation from the corresponding case with a pure electron-positron plasma, shown in the left-hand panel. Such a lepton dominated outflow with $\kappa_e = 1$ starts to accelerate at $5 \times 10^4 r_L$ in the case of the Crab, and converts only 10% of its Poynting flux into kinetic energy before terminating.

In the acceleration phase, where $p_\perp \approx p_{\perp\text{eq}}$, one finds from Eqs. (2) and (25)

$$\begin{aligned} \gamma_i &\approx r / (2\kappa_{\text{ep}} r_L) \\ \gamma_e &\approx \eta_{\text{ion}} \gamma_i, \end{aligned} \quad (29)$$

for the ion dominated case ($\eta_{\text{ion}} \gg 1$), and

$$\gamma_e \approx r / (\kappa_{\text{ep}} r_L), \quad (30)$$

for the lepton dominated case, ($\eta_{\text{ion}} \ll 1$).

At the end of the acceleration phase, the Poynting flux is negligible and the maximum Lorentz factors achieved are given by (15), setting $\Psi_{\text{Poynting}} \rightarrow 0$, leading to

$$\begin{aligned} \gamma_{i,\text{max}} &\approx a_{Li} / (4\kappa_i) \\ \gamma_{e,\text{max}} &\approx a_{Le} / (4\kappa_{\text{ep}}) \end{aligned} \quad (31)$$

for $\eta_{\text{ion}} \gg 1$ and

$$\begin{aligned}\gamma_{i,\text{max}} &= a_{\text{Li}} / \left(2\sqrt{2}\kappa_i\right) \\ \gamma_{e,\text{max}} &= a_{\text{Le}} / (2\kappa_{\text{ep}})\end{aligned}\quad (32)$$

for $\eta_{\text{ion}} \ll 1$. These estimates hold provided $\kappa_i > 1$ and $\kappa_{\text{ep}} > 1$ — see the discussion of the range of validity of the fluid approximation in § 5. The radius at the end of the acceleration zone follows from (29) and (30):

$$r_{\text{max}} \approx a_{\text{Le}} r_{\text{L}} / 2 (1 + \eta_{\text{ion}}), \quad (33)$$

showing that conversion of electromagnetic energy into particle energy takes place much more rapidly when ions dominate.

For $r > r_{\text{max}}$, the flow enters a coasting phase, in which, according to the equations derived here, the leptons relax to the same Lorentz factor as the ions, and the flow subsequently proceeds at constant velocity in the absence of the wave component of the fields. However, as we discuss below, the validity of the perturbation expansion underlying this description is doubtful when $r \gtrsim \kappa_{e,i} r_{\text{max}}$.

5. DISCUSSION

The solutions presented in § 4 are based on a perturbation analysis of the multi-fluid equations, using the small parameter r_{L}/r . This results in a simple, closed system of equations describing the radial evolution of the zeroth-order quantities in a quasi-stationary, Poynting-flux dominated flow, once it has left the vicinity of the rotating, magnetized object that launches it. The nature of the first-order fields plays no role, provided only that they remain small compared to the zeroth-order fields. They may, for example, be rapidly oscillating functions of wave phase. In principle, solutions could be found analytically for these quantities. However, even within this restricted, multi-fluid description, the number of degrees of freedom available to the plasma is considerable, and the choice of initial conditions largely unconstrained, so that it would be difficult to extract additional insights from particular, first-order solutions.

Alternatively, the multi-fluid equations could be solved numerically without recourse to perturbation theory. Several groups have developed appropriate algorithms, and applied them to special situations, such as a reconnecting current sheet, or a Poynting-flux dominated termination shock (Zenitani et al. 2009; Kojima & Oogi 2009; Amano & Kirk 2013; Barkov & Komissarov 2016; Amano 2016). The results reveal structures similar to those observed in particle-in-cell simulations, which, at least in principle, incorporate more of the microphysics. However, the multi-fluid algorithms introduce arbitrary dissipative terms such as

viscosity and resistivity, that are absent in the model with cold fluids presented here, and that might mask the importance of the inertial effects responsible for inductive acceleration.

In the perturbative approach, the zeroth-order electric field is orthogonal to the zeroth-order fluid velocity, and acceleration is the result of higher order effects associated with the motion of cold fluids, which, to this order, are no longer tied to magnetic field lines. This picture fails at the microscopic level if the fluids do not remain cold, or if the flow contains too few particles for them to be represented as fluids. In the following we discuss these limitations in turn.

5.1. Dissipation and magnetic reconnection

The cold fluid assumption breaks down if instabilities result in the dissipation a significant amount of energy into heat. The sheet pinch equilibrium assumed in § 3 is stable within the ideal MHD description. Furthermore, it is not subject to the kinetic tearing mode instability, since the corresponding growth rate vanishes for a cold plasma. Nevertheless, counter-streaming electron and positron fluids are subject to a Buneman-type electrostatic instability (Li et al. 2003), which leads to randomization of the component of the leptonic velocity along the local magnetic field. The instability saturates when the velocity dispersion reaches the drift speed cp_{\perp}/γ_e , which is small in the MHD regime, but could, in principle, lead to an anomalous resistivity, and the destabilization of the tearing mode (Komissarov et al. 2007). In this case the subsequent nonlinear evolution generates a turbulent magnetic field component of the same order of magnitude as the regular component, as confirmed by numerous simulations (for a recent review, see Kagan et al. 2015).

The growth rate of the electrostatic instability, seen in the frame co-moving with the wave (the “wave frame”), is of the order of the proper plasma frequency, ω_p . Assuming this growth is sufficiently rapid, the subsequent reconnection rate is limited from above by the rate at which the particle distribution can be isotropized, i.e., by the gyro-frequency ω_g of an electron of four-velocity p_{\perp} moving in the magnetic field $|B|/\gamma_w$ seen in the wave frame:

$$\begin{aligned}\omega_g &= \frac{e|B|}{\gamma_w \sqrt{1 + p_{\perp}^2} m_e c} \\ &= \frac{\omega a_{\text{Le}} r_{\text{L}}}{\gamma_e r}.\end{aligned}\quad (34)$$

To assess whether or not dissipation is possible, these rates must be compared to the dynamical rate of evolu-

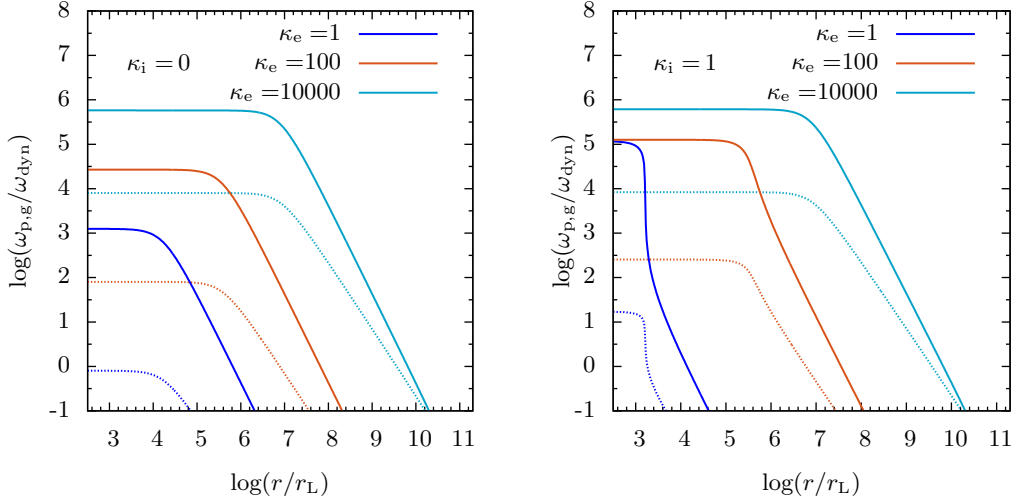


Figure 2. Ratios of the proper plasma frequency ω_p (dotted lines) and the electron gyro frequency ω_g (solid lines) to the dynamical expansion rate ω_{dyn} (see Eqs. (36) and (37)) for the solutions presented in Fig. 1.

tion imposed by expansion of the flow

$$\omega_{\text{dyn}} = \gamma_w c / r, \quad (35)$$

which is measured in the wave frame at fixed phase. Using Eq. (9), one finds

$$\frac{\omega_p}{\omega_{\text{dyn}}} \approx \frac{(2a_{\text{Le}}\kappa_{\text{ep}})^{1/2}}{\gamma_w^{3/2} (1 + p_{\perp}^2)^{1/4}} \quad (36)$$

and

$$\frac{\omega_g}{\omega_{\text{dyn}}} \approx \frac{a_{\text{Le}}}{\gamma_w^2 (1 + p_{\perp}^2)^{1/2}}. \quad (37)$$

Figure 2 depicts these ratios for the illustrative cases discussed in § 4 and shown in Fig. 1. During the MHD phase, both $\omega_p/\omega_{\text{dyn}}$ and $\omega_g/\omega_{\text{dyn}}$ remain constant and greater than unity for all cases studied except for the low density, pair plasma case $\kappa_i = 0$, $\kappa_e = 1$, where $\omega_p/\omega_{\text{dyn}} \approx 1$. This does not establish the importance of dissipation in the MHD phase, but it also does not rule it out. More importantly, the relevance of microphysical processes declines rapidly when the acceleration phase is entered, and both rates drop below the dynamical expansion rate at some point before acceleration is complete, provided the lepton density in the wind is sufficiently low. Inserting the expressions for γ_{max} , Eq. (31) into (36) and (37) one finds that ω_p and ω_g drop below the expansion rate before the end of the acceleration phase if

$$\kappa_e \lesssim \sqrt{a_{\text{Le}} / \text{Max}(\eta_{\text{ion}}, 1)} \approx 10^5 (4\pi L_{38} / \Omega)^{1/4} / \text{Max}(\eta_{\text{ion}}^{1/2}, 1), \quad (38)$$

which confirms the point previously made by Lyubarsky & Kirk (2001, see their Eq. (37)).

Several groups have analyzed Poynting-flux dominated flows assuming, on the contrary, that dissipation by reconnection is important (Lyubarsky & Kirk 2001; Drenkhahn & Spruit 2002; Drenkhahn 2002; Kirk & Skjæraasen 2003; Lyubarsky 2010; Bégué et al. 2017; Giannios & Uzdensky 2019). The existence of a hot current sheet that can be described by an isotropic pressure tensor is implicit in all of these investigations, but different prescriptions are used to specify the dissipation rate. In each case, bulk acceleration of the flow is found: $\gamma_w \propto r^q$, typically with $q \sim 1/3$ to $1/2$. However, for low density winds, Eq. (38) shows that acceleration inevitably leads into a regime in which dissipation is frozen out before it is complete, and it is reasonable to expect that the evolution subsequently proceeds as in the inductive solutions presented in § 4.

Without making assumptions about the dissipation and isotropization rates, several sets of PIC simulations have demonstrated that magnetic structures frozen into a Poynting-flux dominated wind do indeed dissipate (Pétri et al. 2015; Zrake 2016; Zrake & Arons 2017; Alves et al. 2018). However, these simulations are limited to small spatial regions, in which the expansion of the flow is neglected. They are, therefore, relevant only to high density flows which are able to dissipate a substantial fraction of their electromagnetic energy before the microphysical processes freeze out. Global simulations (Cerutti & Philippov 2017) offer a more generally applicable approach, but they are expensive in terms of computing resources. To date, they have been used to study the launch of only relatively weak waves, and do not yet extend into the acceleration phase predicted in § 4.

5.2. The fluid approximation and the Hillas Limit

Assuming an undisturbed flow, the maximum Lorentz factor achieved in the current model, given by Eq. (31), is inversely proportional to the multiplicities. Since a fluid description is used, this expression must break down at sufficiently small multiplicity, when there are too few particles for the star to launch a wind that can be described by the MHD equations. Exactly when this happens is unclear. One plausible constraint for ensuring fluid behavior is $\kappa_{e,i} \gtrsim 1$, since, when this is violated, superluminal waves are able to propagate at $r > r_L$ (Mochol & Kirk 2013) and could be launched in place of the MHD flow. As a consistency check on this constraint, the magnitude of the phase-averaged, first-order effects responsible for acceleration can be estimated by ascribing them to an effective radial electric field $E_{e,i}^{(1)}$, defined as

$$E_{e,i}^{(1)} = \frac{m_{e,i} c^2}{|q_{e,i}|} \frac{d\gamma_{e,i}}{dr}. \quad (39)$$

Then, from Eq. (25), noting that p_\perp is constant during the acceleration phase,

$$E_{e,i}^{(1)} / |B| \approx r / (r_{\max} \kappa_{e,i}). \quad (40)$$

Therefore, the perturbation approach loses validity when when r approaches $\kappa_{e,i} r_{\max}$ and the choice $\kappa_{e,i} > 1$ ensures that this does not happen until the flow has entered the final coasting phase.

It is interesting to compare the limit implied jointly by Eq. (31), together with the choice $\kappa_{e,i} > 1$, with the limit on rigidity, R_H , given by Hillas (1984): $R_H < (v/c)^2 \bar{B} \bar{r}$, where \bar{r} and \bar{B} are a characteristic length and magnetic field strength, and v is a bulk flow velocity. These limits coincide if v is assumed to be close to c , and \bar{B} is interpreted as the amplitude $|B|$ of the oscillating, zeroth-order field in the wind at radius $r = \bar{r}$. In our case, the limit is not strict, since it is imposed by the range of validity of the approximations employed. In particular, our treatment formally leaves open the possibility that instabilities in flows with $\kappa_{e,i} < 1$ might accelerate particles to higher rigidity. However, to do this, the flow must generate fields at large radius whose strength exceeds that of the decaying wave component, placing it out of reach of our perturbative description. Of course, if \bar{B} is reinterpreted in terms of these amplified fields, the Hillas limit remains valid.

5.3. Radiation losses

To zeroth order in the small parameter r_L/r , the acceleration suffered by the charged fluids in these solutions vanishes. Furthermore, first-order acceleration in the

effective, phase-averaged electric field given by (40) is parallel to the zeroth-order fluid velocity, which severely reduces the radiation losses. Nevertheless, it is reasonable to expect that phase-dependent components of the electromagnetic fields perpendicular to the fluid velocity might also exist and be of similar magnitude. In this case, a rough estimate of the energy loss rate by radiation of the lepton fluids can be found from Larmor's formula:

$$\begin{aligned} \omega_{\text{loss}} &= \frac{1}{\gamma_e} \frac{d\gamma_e}{dt} \\ &= \frac{2e^4}{3m_e^3 c^5} \gamma_e \left(E_e^{(1)} \right)^2 \end{aligned} \quad (41)$$

In most cases, the corresponding radiation process is synchrotron radiation, although it should be noted that Larmor's formula is quite general, remaining valid even for motion in rapidly oscillating electromagnetic fields, a process sometimes referred to as *jitter* radiation. Inserting the estimate given in (39) and dividing the resulting loss rate by the dynamical expansion rate gives

$$\frac{\omega_{\text{loss}}}{\omega_{\text{dyn}}} = \left(\frac{2e^2 \omega}{3mc^3} \right) \left(\frac{r_L \gamma_e^2 \sqrt{1+p_\perp^2}}{r} \right) \left(\frac{r}{\gamma_e} \frac{d\gamma_e}{dr} \right)^2 \quad (42)$$

In the acceleration region, where $\gamma_e \propto r$, losses become progressively more important at larger radius, and, at $r \approx r_{\max}$, one has, to order of magnitude,

$$\begin{aligned} \frac{\omega_{\text{loss}}}{\omega_{\text{dyn}}} &\approx \frac{2e^4}{3m_e^3 c^5} \text{Max}(1, \eta_{\text{ion}}^2) a_e \\ &\approx 10^{-13} \text{Max}(1, \eta_{\text{ion}}^2) L_{38}^{1/2} P_{\text{sec}}^{-1}, \end{aligned} \quad (43)$$

where P_{sec} is the wave period expressed in seconds. Thus, radiation losses in the acceleration zone are negligible for pulsars, but could enter into play in the distant regions of a flow driven by a protomagnetar, where $L_{38} \approx 10^{16}$ and $P_{\text{sec}} \approx 10^{-3}$ (Metzger et al. 2011).

In the inner parts of the flow, the transition from the MHD to the acceleration zone produces rapid energization of the leptons, in particular if ions dominate the rest-mass flux. From (27) one can estimate that, for $\eta_{\text{ion}} \gg 1$, $d \ln \gamma_e / d \ln r \sim \eta_{\text{ion}} / p_\perp$ in the zone close to $r = r_{\text{MHD}}$, and, therefore,

$$\begin{aligned} \frac{\omega_{\text{loss}}}{\omega_{\text{dyn}}} &\approx \left(\frac{2e^2 \omega}{3mc^3} \right) \eta_{\text{ion}}^{8/3} \kappa_{\text{ep}}^{-4/3} a_{\text{Le}}^{1/3} \mathcal{M}^{2/3} \\ &\approx 10^{-19} \eta_{\text{ion}}^{8/3} \kappa_{\text{ep}}^{-4/3} \mathcal{M}^{2/3} L_{38}^{1/6} P_{\text{sec}}^{-1}. \end{aligned} \quad (44)$$

Radiation losses in this part of the flow are, therefore, dynamically unimportant, unless the wind is launched at a very high Mach number. However, this statement applies only to losses caused by the electromagnetic fields

carried by the wind. Other mechanisms, such as inverse Compton scattering off the ambient photon field, could, in principle, be important in objects such as protomagnetars, blazars and in the phenomena powering gamma-ray bursts.

5.4. Migration in latitude and the unipolar inductor

In addition to the limitations placed on the model by microphysical effects, another potential limitation arises at the global level, because of the assumption that the flow is uniform and radial within a solid angle Ω . Since $p_{\perp s}/p_{\parallel s} \leq (\beta_w \gamma_w)^{-1} \ll 1$, the fluid trajectories indeed remain radial to a good approximation. However, as an individual fluid element moves outwards, its radius vector drifts slowly in latitude and/or longitude — depending on the wave phase at which it is located — implying that the assumption of uniformity within Ω is valid only if the angular displacement $\Delta\theta$ accumulated by each element between launch and $r = r_{\max}$ satisfies $\Delta\theta < \Omega^{1/2}$. The rate at which the radius vector rotates is given by

$$\frac{d\theta}{dr} = \frac{p_{\perp \text{eq}}}{r\gamma_e} \quad (45)$$

$$\approx \frac{1}{r\gamma_w} \quad (46)$$

for $p_{\perp \text{eq}} \geq 1$. Integrating over the entire acceleration phase, one finds an accumulated displacement of $\Delta\theta = 2\kappa_{\text{ep}} r_L / r_{\text{MHD}}$. A uniform flow requires $\Omega > \Delta\theta^2$, which corresponds to $\Omega \gtrsim \gamma_{w0}^{-2}$. Thus, the angular displacement or spreading of the beam is small and a uniform, radial flow is a good approximation provided the conditions at launch are homogeneous on angular scales smaller than $\mathcal{M}^{-1}\sigma_0^{-1}$.

The situation is different in models which extract energy from the static component of the magnetic field, such as that proposed by Bell (1992), or the closely related “unipolar inductor” model (Blasi et al. 2000; Arons 2003). There, the electric field responsible for acceleration can be described by an electrostatic potential with conical equipotential surfaces of constant latitude. Therefore, particles are accelerated only if their trajectories migrate in latitude, and the Hillas limit is reached by charges that drift all the way from the equator to the pole (or vice-versa). These models have been developed by computing test-particle trajectories in the fields given by solutions of the force-free equations. So far, they do not address the back reaction of the charge separation and currents implied by the particle flows on the original fields. Therefore, unlike the solutions presented in Fig. 1, they do not provide a self-consistent explanation of how Poynting flux is converted into the power carried by accelerated particles.

6. CONCLUSIONS

Inductive acceleration in a Poynting-flux dominated, relativistic outflow is a viable mechanism for accelerating not only leptons, but also ions up to energies close to the limiting value given by Hillas (1984). The solutions given in § 4, and illustrated in Fig. 1, explicitly describe the rate of particle acceleration and the accompanying depletion of Poynting flux, and demonstrate that, in the presence of ions, comparable power is channeled into the leptonic and ionic components. These solutions provide a self-consistent theoretical basis for the idea that objects such as newly born magnetars and pulsars are potential sources of ultra-high energy cosmic rays, an hypothesis whose implications were explored in detail by Blasi et al. (2000) and Arons (2003).

The leptonic version of inductive acceleration has previously been applied to both blazar jets (Kirk & Mochol 2011a) and pulsar wind nebulae (Kirk & Giacinti 2017). In each case, the primary limitation on the maximum possible particle energy is imposed by the finite size of the region traversed by the unperturbed relativistic flow, before it is terminated by the surrounding medium. Introducing ions into the flow exerts a confining effect on the leptons, enabling them to reach a given energy in a much shorter distance. Thus, in the case of blazars, the presence of ions moves the location of the acceleration zone in from ~ 1 pc to ~ 0.1 pc, placing it inside the region where broad emission lines are thought to originate. In the case of the pulsar wind nebulae that surround the Crab pulsar and the powerful pulsars B0450–69 and J0537–6910, the presence of ions raises the expected energy with which leptons can be injected into the nebula by roughly one order of magnitude. In contrast to the related unipolar inductor model, both purely leptonic flows and flows containing ions remain tightly collimated in the radial direction during the acceleration process. Radiation losses via synchrotron or jitter radiation are shown in § 5.3 to be unimportant for the dynamics of the flow except, perhaps, in the case of protomagnetars. Losses by inverse Compton scattering off ambient photons may be more important, depending on the environment in which the flow is accelerating, but we leave a discussion of the observational implications of such effects to future work.

Inductive acceleration is based on the assumption that the energy contained in the magnetic fluctuations carried by an expanding outflow is channeled directly into bulk kinetic energy, rather than first being released by a dissipative mechanism such as magnetic reconnection. In § 5.1 it is shown that dissipation is too slow to be important in flows with an electron multiplicity $\kappa_e \lesssim 10^5 (4\pi L_{38}/\Omega)^{1/4} / \text{Max}(\eta_{\text{ion}}^{1/2}, 1)$, in which case in-

ductive acceleration indeed dominates. Although this expression is derived in spherical geometry, the generic nature of the mechanism suggest that a similar limit applies to other low-density, Poynting-dominated, expanding flows, such as those thought to be present in the jets of active galactic nuclei and in gamma-ray bursts sources.

ACKNOWLEDGMENTS

We thank Damien Bégué, Uri Keshet, Yuri Lyubarsky and Brian Reville for helpful discussions. This research was supported by a Grant from the GIF, the German-Israeli Foundation for Scientific Research and Development.

Software: Wolfram Research, Inc., Mathematica, Version 11.0, Champaign, IL (2016)

REFERENCES

- Alves, E. P., Zrake, J., & Fiuza, F. 2018, *PhRvL*, 121, 245101, 1810.05154
- Amano, T. 2016, *ApJ*, 831, 100, 1607.08487
- Amano, T., & Kirk, J. G. 2013, *ApJ*, 770, 18, 1303.2702
- Arons, J. 2003, *ApJ*, 589, 871, astro-ph/0208444
- Barkov, M. V., & Komissarov, S. S. 2016, *MNRAS*, 458, 1939, 1602.02848
- Bégué, D., Pe'er, A., & Lyubarsky, Y. 2017, *MNRAS*, 467, 2594, 1610.03673
- Bell, A. R. 1992, *MNRAS*, 257, 493
- Blasi, P., Epstein, R. I., & Olinto, A. V. 2000, *ApJ*, 533, L123, astro-ph/9912240
- Bobrova, N. A., Bulanov, S. V., Sakai, J. I., & Sugiyama, D. 2001, *Physics of Plasmas*, 8, 759
- Bogovalov, S. V. 1999, *A&A*, 349, 1017, arXiv:astro-ph/9907051
- Buckley, R. 1977, *MNRAS*, 180, 125
- Bühler, R., & Blandford, R. 2014, *Reports on Progress in Physics*, 77, 066901, 1309.7046
- Cerutti, B., & Philippov, A. A. 2017, *A&A*, 607, A134, 1710.07320
- Contopoulos, I., & Kazanas, D. 2002, *ApJ*, 566, 336, astro-ph/0110183
- Contopoulos, I., Kazanas, D., & Fendt, C. 1999, *ApJ*, 511, 351, astro-ph/9903049
- Coroniti, F. V. 1990, *ApJ*, 349, 538
- Drenkhahn, G. 2002, *A&A*, 387, 714, arXiv:astro-ph/0112509
- Drenkhahn, G., & Spruit, H. C. 2002, *A&A*, 391, 1141, arXiv:astro-ph/0202387
- Gao, S., Fedynitch, A., Winter, W., & Pohl, M. 2019, *Nature Astronomy*, 3, 88, 1807.04275
- Giannios, D., & Uzdensky, D. A. 2019, *MNRAS*, 484, 1378, 1805.09343
- Goldreich, P., & Julian, W. H. 1970, *ApJ*, 160, 971
- Hillas, A. M. 1984, *Annual Review of Astronomy and Astrophysics*, 22, 425
- IceCube Collaboration et al. 2018, *Science*, 361, eaat1378, 1807.08816
- Kagan, D., Sironi, L., Cerutti, B., & Giannios, D. 2015, *SSRv*, 191, 545, 1412.2451
- Kirk, J. G., & Giacinti, G. 2017, *PhRvL*, 119, 211101
- Kirk, J. G., Lyubarsky, Y., & Petri, J. 2009, in *Astrophysics and Space Science Library*, Vol. 357, *Astrophysics and Space Science Library*, ed. W. Becker, 421, arXiv:astro-ph/0703116
- Kirk, J. G., & Mochol, I. 2011a, *ApJ*, 729, 104, arXiv:1012.0307
- . 2011b, *ApJ*, 736, 165
- Kirk, J. G., & Skjæraasen, O. 2003, *ApJ*, 591, 366, arXiv:astro-ph/0303194
- Kojima, Y., & Oogi, J. 2009, *MNRAS*, 398, 271, 0905.3468
- Komissarov, S. S., Barkov, M., & Lyutikov, M. 2007, *MNRAS*, 374, 415, astro-ph/0606375
- Kotera, K., & Olinto, A. V. 2011, *Annual Review of Astronomy and Astrophysics*, 49, 119, 1101.4256
- Lemoine, M. 2013, in *Journal of Physics Conference Series*, Vol. 409, *Journal of Physics Conference Series*, 012007, 1209.6442
- Li, H., Nishimura, K., Barnes, D. C., Gary, S. P., & Colgate, S. A. 2003, *Physics of Plasmas*, 10, 2763
- Lyubarsky, Y. 2010, *ApJL*, 725, L234, 1012.1411
- Lyubarsky, Y., & Kirk, J. G. 2001, *ApJ*, 547, 437, arXiv:astro-ph/0009270
- Metzger, B. D., Giannios, D., Thompson, T. A., Bucciantini, N., & Quataert, E. 2011, *MNRAS*, 413, 2031, 1012.0001
- Michel, F. C. 1969, *ApJ*, 158, 727
- Mochol, I., & Kirk, J. G. 2013, *ApJ*, 771, 53, 1303.6434
- Pétri, J., Takamoto, M., Baty, H., & Zenitani, S. 2015, *Plasma Physics and Controlled Fusion*, 57, 014034
- Petropoulou, M., & Mastichiadis, A. 2018, *MNRAS*, 477, 2917, 1804.00188

- Reimer, A., Boettcher, M., & Buson, S. 2018, arXiv e-prints, arXiv:1812.05654, 1812.05654
- Usov, V. V. 1975, *Ap&SS*, 32, 375
- Werner, G. R., Uzdensky, D. A., Begelman, M. C., Cerutti, B., & Nalewajko, K. 2018, *MNRAS*, 473, 4840, 1612.04493
- Zacharias, M., Böttcher, M., Jankowsky, F., Lenain, J. P., Wagner, S. J., & Wierzcholska, A. 2019, *ApJ*, 871, 19, 1811.12299
- Zenitani, S., Hesse, M., & Klimas, A. 2009, *ApJ*, 696, 1385, 0902.2074
- Zrake, J. 2016, *ApJ*, 823, 39, 1512.05426
- Zrake, J., & Arons, J. 2017, *ApJ*, 847, 57, 1612.02430